JGR Atmospheres

RESEARCH ARTICLE
10.1029/2019JD032099

Key Points:
- The propagation effect of NBEs is analyzed using full-wave model and compared with measurement
- The simplified ray-theory method might require correction comparing to the full-wave model
- We quantify errors in the ionospheric height evaluated from the Smith method

Correspondence to:
D. Li,
dsl@iaa.es

Citation:
Li, D., Liu, F., Pérez-Invernón, F. J., Lu, G., Qin, Z., Zhu, B., & Luque, A. (2020).On the accuracy of ray-theory methods to determine the altitudes of intracloud electric discharges and ionospheric reflections: Application to narrow bipolar events. *Journal of Geophysical Research: Atmospheres*, *125*, e2019JD032099. https://doi.org/10.1029/2019JD032099

Received 21 NOV 2019
Accepted 20 APR 2020
Accepted article online 27 APR 2020

On the Accuracy of Ray-Theory Methods to Determine the Altitudes of Intracloud Electric Discharges and Ionospheric Reflections: Application to Narrow Bipolar Events

Dongshuai Li[1], Feifan Liu[2], F. J. Pérez-Invernón[1,3], Gaopeng Lu[2,4], Zilong Qin[5], Baoyou Zhu[2], and Alejandro Luque[1]

[1]Instituto de Astrofísica de Andalucía (IAA), CSIC, Granada, Spain, [2]CAS Key Laboratory of Geo-space Environment, School of Earth and Space Sciences, University of Science and Technology of China, Hefei, China, [3]Institüt für Physik der Atmosphäre, Deutsches Zentrum für Luft- und Raumfahrt, Wessling, Germany, [4]Key Laboratory for Middle Atmosphere and Global Environment Observation, Institute of Atmospheric Physics, Chinese Academy of Sciences, Beijing, China, [5]Guangdong-Hongkong-Macao Greater Bay Area Weather Research Center for Monitoring Warning and Forecasting (Shenzhen Institute of Meteorological Innovation), Shenzhen, China

Abstract Narrow bipolar events (NBEs) (also called narrow bipolar pulses [NBPs] or compact intracloud discharges [CIDs]) are energetic intracloud discharges characterized by narrow bipolar electromagnetic waveforms identified from ground-based very low frequency (VLF)/low-frequency (LF) observations. The simplified ray-theory method proposed by Smith et al. (1999, https://doi.org/10.1029/1998JD200045; 2004, https://doi.org/10.1029/2002RS002790) is widely used to infer the altitude of intracloud lightning and the effective (or virtual) reflection height of the ionosphere from VLF/LF signals. However, due to the large amount of high-frequency components in NBEs, the propagation effect of the electromagnetic fields for NBEs at large distance depends nontrivially on the geometry and the effective conductivity of the Earth-ionosphere waveguide (EIWG). In this study, we investigate the propagation of NBEs by using a full-wave Finite-Difference Time-Domain (FDTD) approach. The simulated results are compared with ground-based measurements at different distances in Southern China, and we assess the accuracy of the simplified ray-theory method in estimating the altitude of the NBE source and the effective reflection height of the ionosphere. It is noted that the evaluated NBE altitudes have a slight difference of about ±1 km when compared with the full-wave FDTD results, while the evaluated ionospheric reflection heights are found to be bigger than those obtained from FDTD model by about 5 km.

1. Introduction

Narrow bipolar events (NBEs), also called narrow bipolar pulses (NBPs) or compact intracloud discharges (CIDs), are intracloud electrical discharges characterized by narrow bipolar electromagnetic waveforms in ground-based very low frequency (VLF)/low-frequency (LF) observations. Several properties of NBEs stand out when compared to other lightning processes: They exhibit short time durations (10–20 m/s), fast propagation speeds (10^7–10^8 m/s), and strong very high frequency (VHF) radiation, and they typically occur isolated from other electrical activities within a time frame of a few milliseconds, although in many cases NBEs are precursors of a leader process inside the thunderstorm (e.g., Gurevich et al., 2003; Le Vine, 1980; Smith et al., 1999, 2002; Willett et al., 1989). These unique properties have turned NBEs into an active research topic that promises to illuminate the initiation mechanism of lightning in a thunderstorm (Rison et al., 2016). Furthermore, the physical mechanism of NBEs is as yet poorly understood (Arabshahi et al., 2014; Gurevich et al., 2002).

Due to the great difficulty in directly measuring the NBE discharge channel and the intracloud current inside the thundercloud, most studies use the identified groundwave and their reflected skywaves in a ground-based VLF/LF signal to determine the altitude of the intracloud NBE source and the effective (or virtual) reflection height in the *D* region of the ionosphere. Smith et al. (1999) expanded the previous techniques to propose a simplified ray-theory method that considers an elevated intracloud source at a finite altitude. Later, Smith et al. (2004) improved the method by accounting for the Earth's curvature. They found

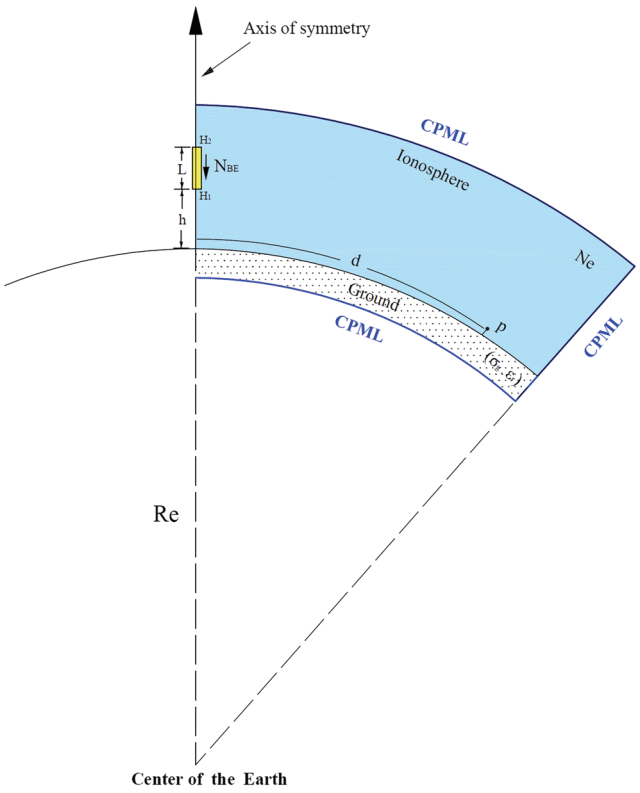

Figure 1. Geometry of the full-wave FDTD model.

that the evaluated ionosphere heights agree well with the expected diurnal variation from 60 to 95 km and with the evaluated NBEs source heights ranging from 7 to 20 km above ground level for positive narrow bipolar events (PNBEs) and for negative narrow bipolar events (NNBEs) occurring above 15 km. This simplified ray-theory method has been applied to many ground-based VLF/LF studies about the altitudes of the PNBEs/NNBEs and the variation of the ionospheric heights in different regions around the world (e.g., Karunarathne et al., 2015; Liu, Zhu et al., 2018; Liu, Zilong et al., 2018; Wu et al., 2012, 2014; Zhang et al., 2016; Zhu et al., 2010). More recently, the altitude of Energetic In-cloud Pulses (EIPs), which are linked to Terrestrial Gamma-ray Flashes (TGFs), has also been evaluated based on this simplified ray-theory method (Lyu et al., 2015, 2016).

Other approaches based on full-wave methods such as wave-hop (ray-theory) method, waveguide mode theory, and the finite-difference time-domain (FDTD) method have also been used to determine the ionospheric height as revealed by ground or intracloud lightning discharges in both daytime and nighttime (e.g., Azadifar et al., 2017; Cummer et al., 1998; Han et al., 2011; Han & Cummer, 2010a, 2010b; Jacobson et al., 2009; Qin et al., 2017; Shao & Jacobson, 2009; Shao et al., 2013; Tran et al., 2017). The propagation effect of NBE electromagnetic pulses or the radiation fields generated by CIDs over finitely conducting ground is mentioned by Rison et al. (2016) and Watson and Marshall (2007), and further investigated by Cooray et al. (2018), but their studies were limited to the groundwave part of the NBE signal. The results show that, due to a large amount of high-frequency components for the narrow features of NBEs, the peak amplitude, the zero-crossing time, the full width at half maximum (FWHM), and the time derivatives of the groundwave of the NBEs were significantly distorted by propagation effects over the finitely conducting ground. However, the propagation effect of the NBEs at far distance in the Earth-Ionosphere WaveGuide (EIWG) will not only depend on the ground conductivity, but it is also a complex function of the geometry and the effective conductivity in the Earth-ionosphere cavity (Smith et al., 1999).

In this paper, we investigate the propagation effect of NBEs by using a full-wave FDTD approach. The simulated results are compared with the ground-based VLF/LF measurements of NBEs at different distances. Moreover, we assess the accuracy of the simplified ray-theory model in evaluating the ionospheric height and the altitude of the NBE source due to the propagation effects of NBEs in the EIWG.

2. Theory and Method

In this section we present a full-wave FDTD model including the propagation effect of the ionospheric reflections and the finitely conducting ground. Note that our FDTD model is very memory and CPU-time intensive due to the large amount of high-frequency components stemming from the narrow features of NBEs. We faced three important challenges: (1) the spatial discretization must be fine enough in comparison with the wavelength (usually 10–20 grid cells per wavelength) in order to make the numerical dispersion error negligible; (2) the time step must be small enough to satisfy the FDTD stability condition; and (3) we are interested in distant fields measured up to several hundred kilometers away from the source. Even though we used the open parallel message passing interface (MPI) technique (Guiffaut & Mahdjoubi, 2001) to improve the FDTD computation efficiency, we were unable to run three-dimensional (3-D) FDTD simulations to solve this large-scale problem. Luckily, the whole FDTD domain is symmetric around the z axis, which allows us to reduce our problem to a two-dimensional (2-D) one by means of symmetry, which vastly reduces the computation and storage required for the simulation. As shown in Figure 1, the geometry of the full-wave FDTD model is based on 2-D spherical coordinates with the sector region defined by the center of the Earth (Bérenger, 2002; Thèvenot et al., 1999).

The FDTD model used in this study solves three fundamental equations as suggested by Marshall (2012) including two Maxwell's curl equations and a modified Ohm equation (sometimes called Langevin equation

Table 1
The NBE Parameters Used for the FDTD Model

Parameters	τ_1 (μs)	τ_2 (μs)	L (m)	h (km)	v (m/s)	σ_g (S/m)	ϵ_r —
Values	1	6	300	10	3.5e7	0.01	10

in this context). In the simulation, only electrons are mobile, since ion motion can be neglected in the lower *D* region ionosphere (Han & Cummer, 2010a) within our time scale of interest. Our system of equations is

$$\epsilon_0 \frac{\partial \vec{E}}{\partial t} = \nabla \times \vec{H} - \vec{J}_e - J_s, \tag{1}$$

$$\mu_0 \frac{\partial \vec{H}}{\partial t} = -\nabla \times \vec{E}, \tag{2}$$

$$\frac{\partial \vec{J}_e}{\partial t} + \nu_e \vec{J}_e = \vec{\omega_{c,e}} \times \vec{J}_e + \omega_{p,e}^2 \epsilon_0 \vec{E}, \tag{3}$$

where J_s is the current density of the source, $\vec{J}_e$ is the self-consistent conduction current driven by the electric field, $\vec{\omega_{c,e}} = e\vec{B}_0/m_e$ is the gyrofrequency vector associated with the geomagnetic field vector $\vec{B}_0$, $\omega_{p,e} = \sqrt{e^2 N_e/m_e\epsilon_0}$ is the plasma frequency, $\nu_e = e/(\mu_e m_e)$ is the collision frequency between electrons and the neutral air, and e, m_e, and N_e are, respectively, the charge, mass, and number density of electrons. The electron mobility μ_e is considered as a function of the local electric field and the background gas number density N_{gas} based on the profile proposed by Pasko et al. (1997). The background gas number density N_{gas} is taken from the MSIS-E-90 model (Hedin, 1991) by assuming a mixed air with 78% N_2 and 22% O_2.

Because we are limited to 2-D symmetrical conditions, the effect of the geomagnetic field is neglected. This is justified according to (Marshall et al., 2010; Marshall, 2012), which claim that the effect of the geomagnetic field can be neglected when its dip angle lies between 0° and 45° in the lower ionosphere, but it can be important for high geomagnetic latitudes. In our case the geomagnetic fields in the campaign region have a dip angle lower than 45°. Note that solar disturbances may influence the geomagnetic field (Han & Cummer, 2010a) but we did not consider that possibility. With this approximation, equation (3) reduces to

$$\frac{\partial \vec{J}_e}{\partial t} + \nu_e \vec{J}_e = \omega_{p,e}^2 \epsilon_0 \vec{E}. \tag{4}$$

Following Wait and Spies (1964), our electron density has an exponential height profile given by

$$N_e = n_e^{ref} e^{\beta(z - H_{ref})}, \tag{5}$$

where β is the steepness of the profile and $n_e^{ref} = 1\text{e}9\ \text{m}^{-3}$ is the electron density where most VLF energy can be reflected at the effective reflected height H_{ref}, which can be evaluated based on the plasma frequency equation $\omega_{p,e} = \sqrt{e^2 N_e/m_e\epsilon_0}$ and the detected bandwidth of the lightning signal.

2.1. FDTD Modeling Parameters

In the FDTD simulation, the computational domain is 500 km × 110 km, with spatial steps of 50 m in both r and z directions. Considering 10 steps per wavelength to avoid the numerical dispersion, the maximum frequency that can be simulated by using our full-wave FDTD model is about 600 kHz, which is enough to cover the VLF/LF frequency band. As shown in Figure 1, we assume a vertical, straight NBE channel above ground and consider the current distribution along the channel according to the modified transmission line model with a linear decay of current with height (MTLL) (Rakov & Dulzon, 1991). The parameters of the NBE current used in this study are based on the VHF observation results from Rison et al. (2016) as shown in Table 1. The NBE current pulse starts at an altitude H_2 and propagates downward at a speed v a distance L to reach the final, lower altitude H_1. At its uppermost point, the NBE current is assumed to follow a double-exponential waveform proposed by Rison et al. (2016):

$$I(t) = I_0 \frac{e^{\alpha t}}{1 + e^{(\alpha+\beta)t}}, \tag{6}$$

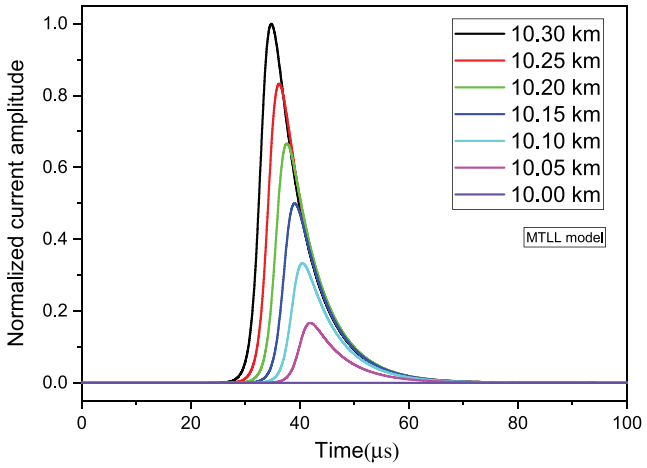

Figure 2. The distribution of the normalized current at different altitude along the NBE channel.

where $\alpha = 1/\tau_1$ and $\beta = 1/\tau_2$ are the rise and fall time constants of the current and the peak current is normalized to one by setting $I_0 = (1 + \frac{\alpha}{\beta})(\frac{\alpha}{\beta})^{(\frac{-\alpha}{\alpha+\beta})}$. Figure 2 shows the distribution of the normalized current at different altitude along the NBE channel.

The observation point p is located at ground level at a distance d from the NBE source. The ground is assumed to be homogeneous with conductivity σ_g and relative permittivity ϵ_r. The ionosphere is considered to be vertically stratified, that is, horizontally homogeneous in the r direction. To avoid artificial reflections at the upper, lower, and outer boundaries of the computational domain, we used absorbing convolutional perfectly matched layers (CPML) (Roden & Gedney, 2000).

2.2. Observation Data

The measured data used in this study were recorded by the Jianghuai Area Sferic Array (JASA) in China. The JASA was established in 2009 to investigate lightning-induced effects in the near-Earth space. It consists of more than 10 LF electric field sensors that continuously record VLF/LF broadband (between 300 Hz and 300 kHz) lightning signals at a sampling rate of 5 MHz with a detection range of up to several thousand kilometers. By using a GPS time receiver with timing accuracy better than 0.1 m/s for each station, the location of an NBE source is obtained by means of the time of arrival (ToA) technique for at least three stations. The location error in the considered area is estimated to better than 2 km (Qin et al., 2015). More details about the measured sensors and instrumentation system can be found in Zhu et al. (2015).

3. Results

During the 2012 campaign, 1,539 NBE events were recorded by JASA including 1,395 positive NBEs and 144 negative NBEs from 4 July to 7 July. Further details about the statistical analysis of all NBE events can be found in Liu et al. (2016). In this study, we focus on one typical positive NBE event captured by JASA at local time 08:57:29 on 7 July 2012. Figure 3 shows a comparison between the simulated waveforms from our full-wave FDTD model and the VLF/LF waveforms for the considered positive NBE event measured at different distances. The typical VLF/LF waveform of NBEs is clearly appreciated in Figure 3, with a groundwave and two ionospheric reflected sky waves marked as G, 1S, and 2S. Notice that, by using the appropriate physical parameters for the Earth and ionosphere, all the simulated results obtained from the full-wave FDTD model agree perfectly with the VLF/LF measurements at distances ranging from about 100 km to about 400 km, thus validating our full-wave FDTD results. The bipolar shape of the electric field waveform is due to the lightning radiation field that is proportional to the time derivative of the current (Uman et al., 1975). Since our measured electric field signal is uncalibrated and the currents of NBEs are not available, the electric fields are normalized to the maximum amplitude measured at different sensors from JASA.

After comparing our FDTD model to the observational results at different distances, let us now compare the FDTD results with the method proposed by Smith et al. (1999, 2004) (henceforth referred to as *Smith method*) to assess the accuracy of this simplified ray-theory method. As mentioned above, this method has been widely used to evaluate the altitude of the intracloud source and the effective (or virtual) reflection height of the D region ionosphere. In the Smith method, the relative times of arrival of the simplified signal reflections between the ground and ionosphere are used to determine both the altitude of the NBE source (h) and the effective (or virtual) reflection height of the ionosphere (H) (see the appendix for the details of the Smith method). As shown in Figure 3a there are several possibilities to calculate the time delays between the groundwave and the first and second sky waves. By T^1_{pp} and T^2_{pp}, we denote the time delay between the positive peaks of both groundwave and reflected skywaves; these are the time delays used in many studies based on the method proposed by Smith et al. (2004). In order to minimize the effect of the noises in the measured data, we applied a moving average filter with a window length of 30 data points to find the negative and positive peaks to determine the time delays. Table 2 lists the altitude of the NBE source (h) and the effective (or virtual) reflection height of the ionosphere (H) evaluated by Smith method based on the time delays T^1_{pp} and T^2_{pp} at different distances as in Figure 3. The table also includes the effective reflected height H_{ref} and the altitude of the NBE source h in the FDTD model. The effective (or virtual) reflection height

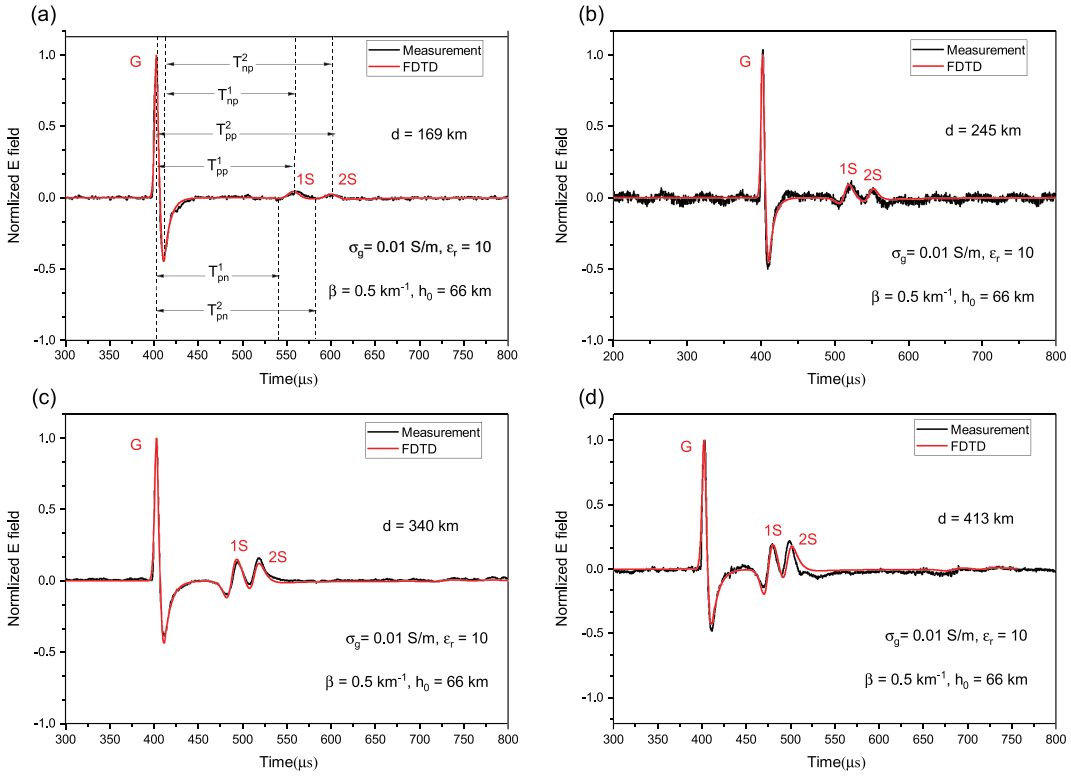

Figure 3. Comparison of normalized electric fields between the simulated FDTD results and the VLF/LF waveforms measured at different sensors from JASA: (a) $d = 169$ km, (b) $d = 245$ km, (c) $d = 340$ km, and (d) $d = 413$ km. The effective reflected height H_{ref} and the steepness β of the profile are 66 km and 0.5 km^{-1}, respectively. The ground conductivity $\sigma_g = 0.01$ S/m and relative permittivity $\epsilon_r = 10$.

of the ionosphere (H) calculated by using Smith method overestimates the effective reflected height in the FDTD simulation (H_{ref}) by about 5 km. The Smith method also overestimates the altitude of NBE source h by about 1 km. This agrees with the comparison results from the VHF radio emission of NBEs observed by the FORTE satellite (Smith et al., 2004). Note that the ground conductivity is assumed to be homogeneous in the model. However, the ground conductivity might be inhomogeneous along the propagation paths to different stations. Figure 4 further shows the influence of the ground conductivity on the electric field at different distances. We see that the finite ground conductivity affects essentially the early time response of the groundwave part of the electric fields by attenuating its peak and slowing down its risetime. Meanwhile, the effect of both groundwave and skywave increases with longer distances. Note that the electric fields for each observation distance are normalized to the maximum amplitude of the case corresponding to perfectly conducting ground ($\sigma_g = \infty$).

Table 2
Altitudes of the NBE Source (h) and the Effective (or Virtual) Reflection Heights of the Ionosphere (H) Evaluated by Smith Method Based on the Different Time Delays of the Measured NBE Waveforms at Different Distances

	(T^1_{pp}, T^2_{pp})		(T^1_{pn}, T^2_{pn})		(T^1_{np}, T^2_{np})	
Distance (km)	H (km)	h (km)	H (km)	h (km)	H (km)	h (km)
169	71.75	10.35	67.05	10.93	66.55	9.93
245	71.87	8.94	67.61	11.26	67.55	10.53
340	71.98	9.62	67.64	10.49	67.50	10.84
413	70.70	9.51	66.51	10.78	67.28	11.02
FDTD	H_{ref} (km)	h (km)	H_{ref} (km)	h (km)	H_{ref} (km)	h (km)
—	66	10	66	10	66	10

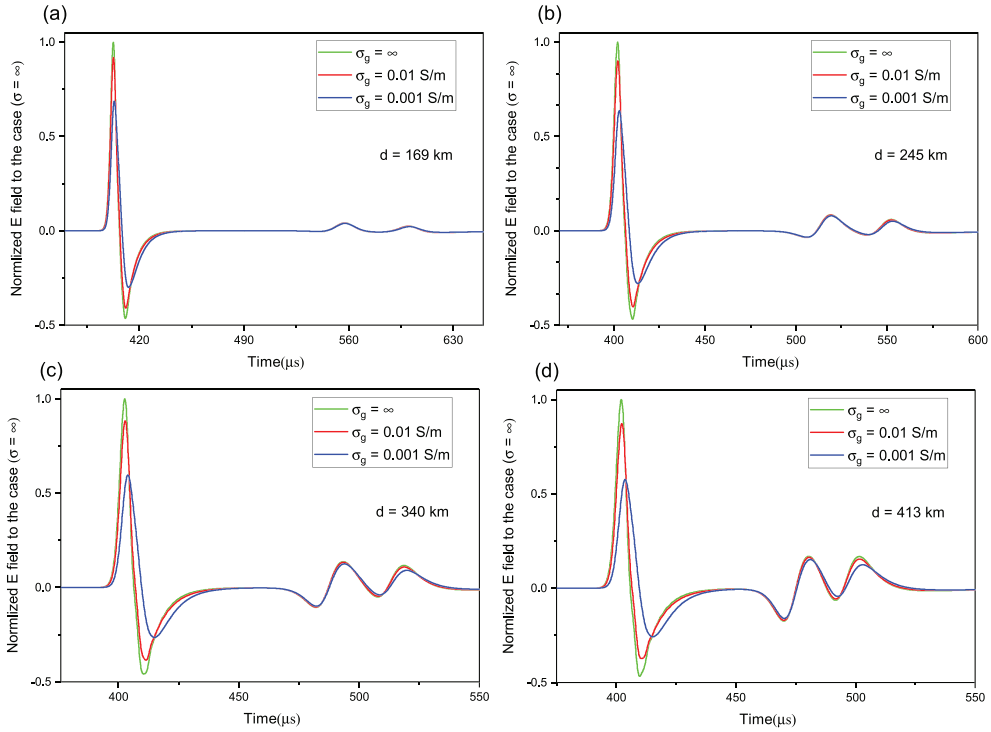

Figure 4. The simulated electric fields by considering different ground conductivities: (i) $\sigma_g = \infty$, (ii) $\sigma_g = 0.01$ S/m, and (iii) $\sigma_g = 0.001$ S/m at different observation distances: (a) $d = 169$ km, (b) $d = 245$ km, (c) $d = 340$ km, and (d) $d = 413$ km. The relative permittivity was set to $\epsilon_{rg} = 10$ in all cases. The effective reflected height H_{ref} and the steepness β of the profile are 66 km and 0.5 km^{-1}, respectively.

Figure 5 further compares the full-wave FDTD results with the geometric ray path of Smith method (see equations (A1) and (A2) in Appendix A) by using cross-sectional views of the normalized electric fields at different time steps. In the Smith method, the signal is assumed to follow the rule of geometric optics by propagating in straight lines and reflecting ideally on the ground and on an effective (or virtual) ionospheric reflection height (H) (Smith et al., 1999). We see in Figure 5 that these assumptions yield the maximum height reached without significant attenuation by the highest-frequency component. However, the FDTD results show that the full-wave electromagnetic pulses from an NBEs contain different frequency components, which are reflected at different heights in the ionosphere. Actually, from Figure 3, we also see that the reflected skywaves are wider and weaker than the groundwaves. Due to dispersion and attenuation in the ionosphere, the higher-frequency components penetrate deeper than the lower ones and are then rapidly attenuated by the higher conductivity.

Furthermore, Figure 3 shows that waveform of the skywave undergoes a polarity reversal comparing to the groundwave. This is because different frequency components in the VLF/LF broadband (300 Hz to 300 kHz) are reflected at different altitudes due to the dependency of the plasma frequency with the electron density. It is therefore more reasonable to measure time delays between peaks of opposite polarity. We propose two other time delay definitions as shown in Figure 3a: T^1_{np} and T^2_{np} are the time delays between the negative peak of groundwave and the positive peaks of the reflected skywaves; T^1_{pn} and T^2_{pn} are the time delays between the positive peak of groundwave and the negative peaks of the reflected skywaves. Table 2 further lists the altitude of the NBE source (h) and the effective (or virtual) reflection height of the ionosphere (H) evaluated by Smith method based on the time delays T^1_{np}/ T^2_{np} and T^1_{pn}/ T^2_{pn} of the simulated NBE waveforms at different distances. Note that in our case by using the new time delays, both altitudes match the full-wave FDTD results well within ±2 km. Comparing the full-wave FDTD model with the Smith method that considers the new time delays in reverse polarity improves the accuracy of estimated effective (or virtual) reflection height of the ionosphere.

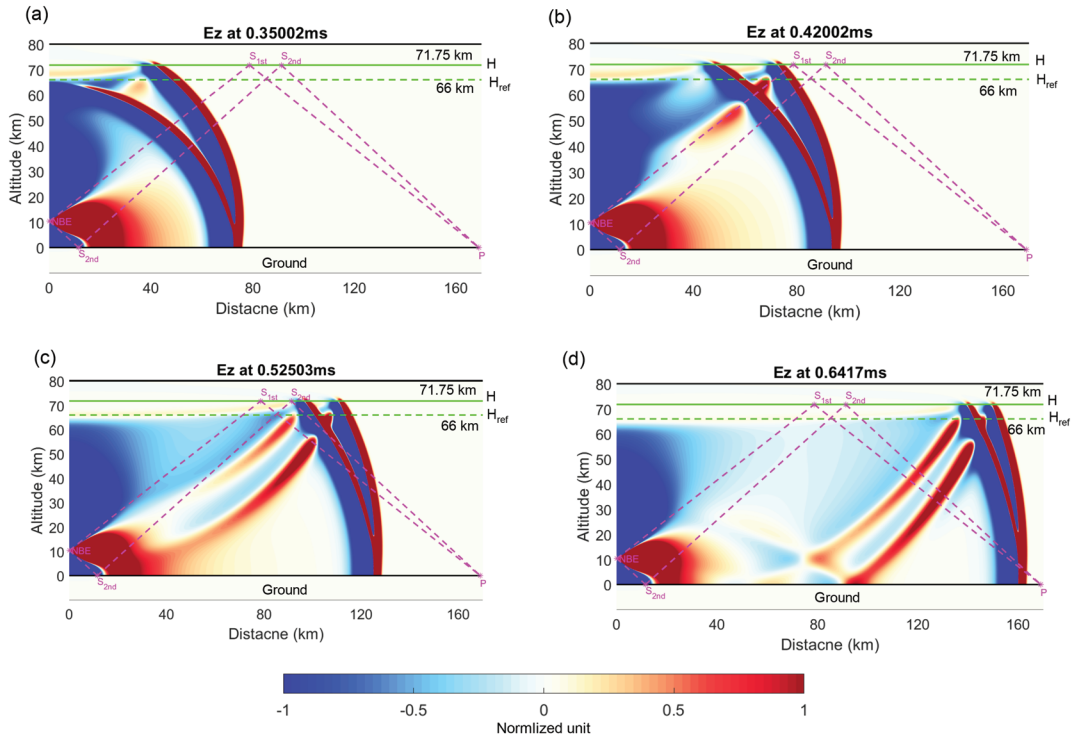

Figure 5. Cross-sectional views of the normalized electric fields for FDTD model associated with the calculated geometric raypath of Smith method at different time steps (a) 0.35002 ms, (b) 0.42002 ms, (c) 0.52503 ms, and (d) 0.6417 ms. The effective (or virtual) reflection height of the ionosphere (H) is calculated by using Smith method, and the effective reflected height (H_{ref}) is obtained from the full-wave FDTD model.

4. Summary and Conclusion

We have investigated the propagation effect of NBEs in the EIWG by using a full-wave FDTD approach. The simulated FDTD results were compared with the ground-based VLF/LF measurements of NBEs from different sensors in Southern China. With the appropriate parameters for the EIWG, the full-wave FDTD results agree perfectly with measurements at distances ranging from about 100 km to about 400 km. Moreover, we assessed the accuracy of the simplified ray-theory model when evaluating the altitude of NBE sources and the ionospheric reflection height. We also proposed different definitions of the time delay between the groundwave and the reflected skywaves in Smith method. We found that considering the new time delays in reverse polarity improves the accuracy of the effective (or virtual) reflection heights of the ionosphere (H); however, by applying the old time delay in the same polarity for Smith method, the evaluated ionospheric reflection heights are found to be larger than the effective reflected heights (H_{ref}) obtained from FDTD model about 5 km. For the altitude of NBE source h, the values from the Smith method have a slight difference of about $\pm$ 1 km when compared with the full-wave FDTD results, which is in agreement with the previous results calculated from the VHF radio emission of NBEs observed by FORTE satellite (Smith et al., 2004).

Appendix A: Simplified Ray-Theory Method Proposed by Smith et al. (1999, 2004)

The simplified ray-theory method proposed by Smith et al. (1999, 2004), which we name Smith method, has been widely used to estimate the altitude of intracloud sources and the reference height of the ionosphere out of ground-based VLF/LF measurements. Figure A1 shows the geometry of the direct groundwave (G) and the first and second reflected skywaves (1S and 2S) generated by an intracloud source inside the EIWG for Smith method. In order to simplify the calculation for the propagation of VLF/LF waves, in the Smith method, the ray path is assumed to follow the rules of geometric optics by propagating in straight paths and being ideally reflected between the ground and an effective (or virtual) ionospheric reflection height (Smith et al., 1999).

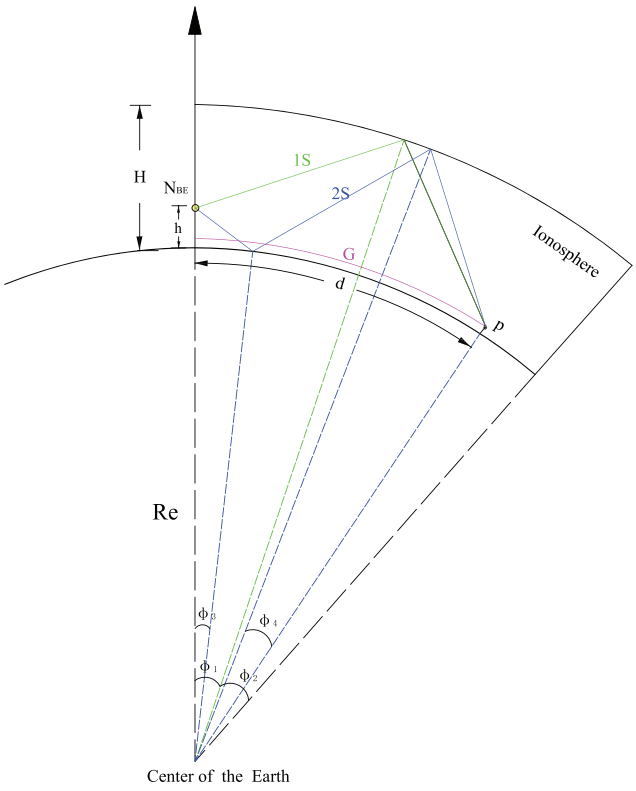

Figure A1. Geometry of the direct groundwave (G) and the first and second reflected skywave (1S and 2S) for an intracloud source in EIWG for Smith method.

The altitude of the NBE source (h) and the effective (or virtual) reflection height of the ionosphere (H) are inferred from the propagation distance (d) and the difference in times of arrival from the direct groundwave and the two reflected skywaves. As shown in Figure A1, the path-length difference d_g^{1s} between the groundwave and first reflected skywave is

$$d_g^{1s} = \sqrt{(R_e+h)^2+(R_e+H)^2-2(R_e+h)(R_e+H)\cos\phi_1} + \sqrt{(R_e+h)^2+R_e^2-2(R_e+h)R_e\cos\phi_2}-d. \tag{A1}$$

Similarly, the path-length difference d_g^{2s} between the groundwave and second reflected skywave is

$$d_g^{2s} = \sqrt{(R_e+h)^2+R_e^2-2(R_e+h)R_e\cos\phi_3}+ 2\sqrt{(R_e+H)^2+R_e^2-2(R_e+H)R_e\cos\phi_4}-d, \tag{A2}$$

where d is the propagation distance between the source and the receiver considering spherical Earth geometry, R_e is the radius of the Earth, and h and H are the altitude of the source and the effective (or virtual) reflection height of the ionosphere. The angles from the Earth's center ϕ_1 to ϕ_4 are shown in Figure A1. Based on equations (A1) and (A2), the altitude of the NBE source (h) and the effective (or virtual) reflection height of the ionosphere (H) can be obtained by using minimum mean square error (MSE) techniques.

Acknowledgments
This work was supported by the European Research Council (ERC) under the European Union H2020 Programme/ERC Grant 681257. The ground-based VLF/LF measurements related to this article can be obtained from CAS Key Laboratory of Geo-space Environment in the School of Earth and Space Sciences at University of Science and Technology of China in Hefei, China (http://222.195.83.28/)

References

Arabshahi, S., Dwyer, J. R., Nag, A., Rakov, V. A., & Rassoul, H. K. (2014). Numerical simulations of compact intracloud discharges as the relativistic runaway electron avalanche-extensive air shower process. *Journal of Geophysical Research: Space Physics*, *119*, 479–489. https://doi.org/10.1002/2013JA018974

Azadifar, M., Li, D., Rachidi, F., Rubinstein, M., Diendorfer, G., Schulz, W., et al. (2017). Analysis of lightning-ionosphere interaction using simultaneous records of source current and 380 km distant electric field. *Journal of Atmospheric and Solar-Terrestrial Physics*, *159*, 48–56.

Bérenger, J.-P. (2002). FDTD computation of VLF-LF propagation in the Earth-ionosphere waveguide. *Annales des télécommunications*, *57*, 1059–1090.

Cooray, V., Fernando, M., Gunasekara, L., & Nanayakkara, S. (2018). Effects of propagation of narrow bipolar pulses, generated by compact cloud discharges, over finitely conducting ground. *Atmosphere*, *9*(5), 193.
Cummer, S. A., Inan, U. S., & Bell, T. F. (1998). Ionospheric D region remote sensing using VLF radio atmospherics. *Radio Science*, *33*(6), 1781–1792.
Guiffaut, C., & Mahdjoubi, K. (2001). A parallel FDTD algorithm using the MPI library. *IEEE Antennas and Propagation Magazine*, *43*(2), 94–103.
Gurevich, A., Duncan, L., Karashtin, A., & Zybin, K. (2003). Radio emission of lightning initiation. *Physics Letters A*, *312*(3-4), 228–237.
Gurevich, A., Duncan, L., Medvedev, Y. V., & Zybin, K. (2002). Radio emission due to simultaneous effect of runaway breakdown and extensive atmospheric showers. *Physics Letters A*, *301*(3-4), 320–326.
Han, F., & Cummer, S. A. (2010a). Midlatitude daytime d region ionosphere variations measured from radio atmospherics. *Journal of Geophysical Research*, *115*, A10314. https://doi.org/10.1029/2010JA015715
Han, F., & Cummer, S. A. (2010b). Midlatitude nighttime d region ionosphere variability on hourly to monthly time scales. *Journal of Geophysical Research*, *115*, A09323. https://doi.org/10.1029/2010JA015437
Han, F., Cummer, S. A., Li, J., & Lu, G. (2011). Daytime ionospheric D region sharpness derived from VLF radio atmospherics. *Journal of Geophysical Research*, *116*, A05314. https://doi.org/10.1029/2010JA016299
Hedin, A. E. (1991). Extension of the MSIS thermosphere model into the middle and lower atmosphere. *Journal of Geophysical Research*, *96*(A2), 1159–1172.
Jacobson, A. R., Shao, X., & Holzworth, R. (2009). Full-wave reflection of lightning long-wave radio pulses from the ionospheric D region: Numerical model. *Journal of Geophysical Research*, *114*, A03303. https://doi.org/10.1029/2008JA013642
Karunarathne, S., Marshall, T. C., Stolzenburg, M., & Karunarathna, N. (2015). Observations of positive narrow bipolar pulses. *Journal of Geophysical Research: Atmospheres*, *120*, 7128–7143. https://doi.org/10.1002/2015JD023150
Le Vine, D. M. (1980). Sources of the strongest RF radiation from lightning. *Journal of Geophysical Research*, *85*(C7), 4091–4095.
Liu, F., Dong, M., Baoyou, Z., Ming, M., & Peng, L. (2016). Characteristics of narrow bipolar events. In *33rd International Conference on Lightning Protection (iclp)*, pp. 1–4. Estoril, Portugal.
Liu, F., Zhu, B., Lu, G., Qin, Z., Lei, J., Peng, K.-M., et al. (2018). Observations of blue discharges associated with negative narrow bipolar events in active deep convection. *Geophysical Research Letters*, *45*, 2842–2851. https://doi.org/10.1002/2017GL076207
Liu, F., Zilong, Q., Baoyou, Z., Ming, M., Mingli, C., & Peng, S. (2018). Observations of ionospheric d layer fluctuations during sunrise and sunset by using time domain waveforms of lightning narrow bipolar events. *Chinese Journal Of Geophysics*, *61*(2), 484.
Lyu, F., Cummer, S. A., Briggs, M., Marisaldi, M., Blakeslee, R. J., Bruning, E., et al. (2016). Ground detection of terrestrial gamma ray flashes from distant radio signals. *Geophysical Research Letters*, *43*, 8728–8734. https://doi.org/10.1002/2016GL070154
Lyu, F., Cummer, S. A., & McTague, L. (2015). Insights into high peak current in-cloud lightning events during thunderstorms. *Geophysical Research Letters*, *42*, 6836–6843. https://doi.org/10.1002/2015GL065047
Marshall, R. A. (2012). An improved model of the lightning electromagnetic field interaction with the d-region ionosphere. *Journal of Geophysical Research*, *117*, A03316. https://doi.org/10.1029/2011JA017408
Marshall, R. A., Inan, U. S., & Glukhov, V. S. (2010). Elves and associated electron density changes due to cloud-to-ground and in-cloud lightning discharges. *Journal of Geophysical Research*, *115*, A00E17. https://doi.org/10.1029/2009JA014469
Pasko, V. P., Inan, U. S., Bell, T. F., & Taranenko, Y. N. (1997). Sprites produced by quasi-electrostatic heating and ionization in the lower ionosphere. *Journal of Geophysical Research*, *102*(A3), 4529–4561.
Qin, Z., Chen, M., Zhu, B., & Du, Y.-P. (2017). An improved ray theory and transfer matrix method-based model for lightning electromagnetic pulses propagating in Earth-ionosphere waveguide and its applications. *Journal of Geophysical Research: Atmospheres*, *122*, 712–727. https://doi.org/10.1002/2016JD025599
Qin, Z., Zhu, B., Ma, M., Ma, D., & Lyu, F. (2015). Using time domain waveforms of return strokes to retrieve the daytime fluctuation of ionospheric d layer. *Chinese Science Bulletin*, *60*(7), 654–663.
Rakov, V. A., & Dulzon, A. (1991). A modified transmission line model for lightning return stroke field calculations. In *Proc. 9th Int. Symp. Electromagn. Compat*, pp. 229–235. Zurich, Switzerland.
Rison, W., Krehbiel, P. R., Stock, M. G., Edens, H. E., Shao, X.-M., Thomas, R. J., et al. (2016). Observations of narrow bipolar events reveal how lightning is initiated in thunderstorms. *Nature Communications*, *7*, 10721.
Roden, J. A., & Gedney, S. D. (2000). Convolution PML (CPML): An efficient FDTD implementation of the CFS-PML for arbitrary media. *Microwave and Optical Technology Letters*, *27*(5), 334–339.
Shao, X.-M., & Jacobson, A. R. (2009). Model simulation of very low-frequency and low-frequency lightning signal propagation over intermediate ranges. *IEEE Transactions on Electromagnetic Compatibility*, *51*(3), 519–525.
Shao, X.-M., Lay, E. H., & Jacobson, A. R. (2013). Reduction of electron density in the night-time lower ionosphere in response to a thunderstorm. *Nature Geoscience*, *6*(1), 29.
Smith, D. A., Eack, K. B., Harlin, J., Heavner, M. J., Jacobson, A. R., Massey, R. S., et al. (2002). The Los Alamos Sferic Array: A research tool for lightning investigations. *Journal of Geophysical Research*, *107*(D13), 4183. https://doi.org/10.1029/2001JD000502
Smith, D. A., Heavner, M. J., Jacobson, A. R., Shao, X. M., Massey, R. S., Sheldon, R. J., & Wiens, K. C. (2004). A method for determining intracloud lightning and ionospheric heights from VLF/LF electric field records. *Radio Science*, *39*, RS1010. https://doi.org/10.1029/2002RS002790
Smith, D. A., Shao, X. M., Holden, D. N., Rhodes, C. T., Brook, M., Krehbiel, P. R., et al. (1999). A distinct class of isolated intracloud lightning discharges and their associated radio emissions. *Journal of Geophysical Research*, *104*(D4), 4189–4212.
Thèvenot, M., Bérenger, J.-P., MonediÈre, T., & Jecko, F. (1999). A FDTD scheme for the computation of VLF-LF propagation in the anisotropic Earth-ionosphere waveguide. *Annales des Télécommunications*, *54*, 297–310.
Tran, T. H., Baba, Y., Somu, V. B., & Rakov, V. A. (2017). FDTD modeling of LEMP propagation in the Earth-ionosphere waveguide with emphasis on realistic representation of lightning source. *Journal of Geophysical Research: Atmospheres*, *122*, 12,918–12,937. https://doi.org/10.1002/2017JD027305
Uman, M. A., McLain, D. K., & Krider, E. P. (1975). The electromagnetic radiation from a finite antenna. *American Journal of Physics*, *43*(1), 33–38.
Wait, J. R., & Spies, K. P. (1964). *Characteristics of the earth-ionosphere waveguide for VLF radio waves*. US Dept. of Commerce, National Bureau of Standards: for sale by the Supt. of Doc., US Govt. Print. Off.
Watson, S. S., & Marshall, T. C. (2007). Current propagation model for a narrow bipolar pulse. *Geophysical Research Letters*, *34*, L04816. https://doi.org/10.1029/2006GL027426
Willett, J. C., Bailey, J. C., & Krider, E. P. (1989). A class of unusual lightning electric field waveforms with very strong high-frequency radiation. *Journal of Geophysical Research*, *94*(D13), 16,255–16,267.

Wu, T., Dong, W., Zhang, Y., Funaki, T., Yoshida, S., Morimoto, T., et al. (2012). Discharge height of lightning narrow bipolar events. *Journal of Geophysical Research*, *117*, D05119. https://doi.org/10.1029/2011JD017054

Wu, T., Yoshida, S., Ushio, T., Kawasaki, Z., Takayanagi, Y., & Wang, D. (2014). Large bipolar lightning discharge events in winter thunderstorms in japan. *Journal of Geophysical Research: Atmospheres*, *119*, 555–566. https://doi.org/10.1002/2013JD020369

Zhang, H., Lu, G., Qie, X., Jiang, R., Fan, Y., Tian, Y., et al. (2016). Locating narrow bipolar events with single-station measurement of low-frequency magnetic fields. *Journal of Atmospheric and Solar-Terrestrial Physics*, *143-144*, 88–101.

Zhu, B., Ma, M., Xu, W., & Ma, D. (2015). Some properties of negative cloud-to-ground flashes from observations of a local thunderstorm based on accurate-stroke-count studies. *Journal of Atmospheric and Solar-Terrestrial Physics*, *136*, 16–22.

Zhu, B., Zhou, H., Ma, M., & Tao, S. (2010). Observations of narrow bipolar events in east china. *Journal of Atmospheric and Solar-Terrestrial Physics*, *72*(2), 271–278.